doi:10.1016/j.jmb.2004.05.059 *J. Mol. Biol.* (2004) **341**, 303–318

JMB

Available online at www.sciencedirect.com

SCIENCE DIRECT®

ELSEVIER

Ligand-induced Assembling of the Type I Interferon Receptor on Supported Lipid Bilayers

Peter Lamken†, Suman Lata†, Martynas Gavutis and Jacob Piehler*

Institute of Biochemistry
Johann Wolfgang
Goethe-University, Biocenter
N210, Marie-Curie-Straße 9
60439 Frankfurt am Main
Germany

Type I interferons (IFNs) elicit antiviral, antiproliferative and immunomodulatory responses through binding to a shared receptor consisting of the transmembrane proteins ifnar1 and ifnar2. Differential signaling by different interferons, in particular IFNαs and IFNβ, suggests different modes of receptor engagement. Using reflectometric interference spectroscopy (RIfS), we studied kinetics and affinities of the interactions between IFNs and the extracellular receptor domains of ifnar1 (ifnar1-EC) and ifnar2 (ifnar2-EC). For IFNα2, we determined a K_D value of 3 nM and 5 μM for the interaction with ifnar2-EC and ifnar1-EC, respectively. As compared to IFNα2, IFNβ formed complexes with ifnar2-EC as well as ifnar1-EC with substantially higher affinity. For neither IFNα2 nor IFNβ was stabilization of the complex with ifnar1-EC in the presence of soluble ifnar2-EC observed. We investigated ligand-induced complex formation with ifnar1-EC and ifnar2-EC being tethered onto solid-supported, fluid lipid bilayers by RIfS and total internal reflection fluorescence spectroscopy. We observed very stable binding of IFNα2 at high receptor surface concentrations with an apparent k_d value approximately 200 times lower than that for ifnar2-EC alone. The apparent k_d value was strongly dependent on the surface concentration of the receptor components, suggesting kinetic stabilization. This was corroborated by the fast exchange of labeled IFNα2 bound to the receptor by unlabeled IFNα2. Taken together, our results indicate that IFN first binds to ifnar2 and subsequently recruits ifnar1 in a transient fashion. In particular, this second step is much more efficient for IFNβ than for IFNα2, which could explain differential activities observed for these IFNs.

Keywords: type I interferon receptor; protein–protein interaction; solid-supported lipid bilayer; reflectometric interference spectroscopy; total internal reflection fluorescence spectroscopy

*Corresponding author

Introduction

Signaling induced by type I interferons (IFNs) plays a key role in host innate response to viral infection by eliciting a pleiotrophic response including antiviral, antiproliferative and immunmodulatory activities. Because of these activities, type I IFNs are attractive for clinical applications in different fields.[1] Although type I interferons are already used successfully in the treatment of several diseases, the complexity of their action interferes with a pharmacologically controlled administration. Thus, better understanding of the receptor recruitment by IFNs and the following downstream events is required for fully exploiting the therapeutical potentials of IFNs.

All type I interferons (13 different IFNαs, 1 IFNβ and 1 IFNω) exert their activity through binding to the same receptor components, ifnar1 and ifnar2.[2] Upon ligand binding, tyrosine kinases associated

† P. L. and S. L. contributed equally to this paper

Abbreviations used: IFN, human type I interferon; ifnar1-EC and ifnar2-EC, extracellular domains of the human type I interferon receptor ifnar1 and ifnar2; wt, wild-type; ifnar2-tl, tag-less ifnar2-EC; NTA, nitrilotriacetic acid; RIfS, reflectometric interference spectroscopy; FRAP, fluorescence recovery after photobleaching; TIRFS, total internal reflection fluorescence spectroscopy; MBP-H10, decahistidine-tagged maltose-binding protein; OG, Oregon green; AF, Alexa Fluor.

E-mail address of the corresponding author: j.piehler@em.uni-frankfurt.de

with the cytoplasmic domains are activated by auto-phosphorylation, followed by phosphorylation of several tyrosine residues on the receptor and other effector molecules, which are mainly members of the STAT family. It appears, however, that the function of different type I IFNs is not fully redundant, and differential signaling by different IFNs has been observed.[3–8] In particular between IFNα subtypes and IFNβ, substantial differences have been observed on the level of receptor phosphorylation[3] and STAT recruitment,[9] as well as on the level of gene induction.[10,11] As so far no further receptor component has been identified, these differences need to be explained through the mode of interaction of IFNs with the extracellular domains of ifnar1 and ifnar2 (ifnar1-EC and ifnar2-EC, respectively). Therefore, a comprehensive structural, biophysical and mechanistic picture of how the receptor domains are recruited in time and space is required for understanding the specificity of signal propagation through the membrane. In the absence of structural data, the recognition of IFNs by the receptor components has been intensively investigated by mutagenesis.[1] The high-affinity interactions between ifnar2-EC and different IFNs have been investigated in detail,[12–14] and a model for the complex between IFNα2 and ifnar2-EC based on double mutant cycle analysis has been reported.[15,16] However, the differences in affinity, binding kinetics and orientation, which have been so far observed for the interaction of IFNα2 and IFNβ with ifnar2-EC are only minute,[13,15,17] and therefore can hardly explain the functional differences. The low-affinity interaction of IFNs with ifnar1 has been much less well characterized and the K_D value was estimated to be in the micromolar range. Compared to cells expressing ifnar2 alone a 10–40-fold decrease in the K_D value has been reported. By using neutralizing antibodies, the binding site for IFNs on ifnar1 was mapped to the Ig-like domains 2 and 3 of ifnar1.[18] This observation was confirmed by several studies with bovine ifnar1,[19,20] which binds human IFNαs with high affinity. These results indicated that the ligand binding site of ifnar1 does not correspond to a classical cytokine binding module. *In vitro*, a stable ternary complex of IFNβ with ifnar1-EC and ifnar2-EC was observed by size-exclusion chromatography.[21] As no stable complex between IFNβ and ifnar1-EC was detectable under these conditions, this result indicated that cooperative interaction leads to stabilization of the ternary complex. For members of the class I cytokine family, contacts between the two extracellular receptor domains apparently contribute to the stability of the ternary complex,[22–26] and pre-association of the receptor chains has been proposed for several receptors.[25,27,28] For the IFNγ-receptor as a member of the class II cytokine receptor family, a similar mechanism was suggested recently.[29] However, the role of stem–stem contacts between the extracellular receptor domains has not been clearly resolved so far, because lateral interactions between membrane-anchored proteins are difficult to study: cellular assays with the full-length receptors do not provide the experimental control required for analyzing inter-receptor interactions properly; binding studies with the extracellular receptor domains in solution do not provide the biophysical constraints of protein–protein interaction within biological membranes such as the reduced number of degrees of freedom (reduced dimensionality) and the reduced diffusion rates.[30]

Here, we have analyzed the interactions at the extracellular domains of ifnar involved in the formation of the active ternary complex for both IFNα2 and IFNβ. We furthermore present a novel approach for studying ligand-induced receptor assembling by combining full experimental control of an *in vitro* reconstituted system with mimicking two-dimensional protein–protein interactions within the plane of the plasma membrane. Through their C-terminal histidine tags, we tethered ifnar1-EC and ifnar2-EC in an oriented manner onto supported fluid lipid bilayers containing lipids carrying high-affinity chelator head groups. We evaluated the interaction of IFNs to the receptor components reconstituted on fluid lipid bilayers by reflectometric interference spectroscopy (RIfS) and total internal reflection fluorescence spectroscopy (TIRFS). Based on these results, we discuss a biophysical model of the ternary complex formation and for differential receptor recruitment by IFNs.

Results

Expression and purification of ifnar1-EC

Ifnar1-EC with a C-terminal decahistidine-tag was expressed in *Sf*9 cells infected with a baculovirus harboring the gene of mature ifnar1-EC fused to the secretion sequence of the baculoviral protein gp67. The protein was purified to homogeneity from the supernatant by IMAC and size-exclusion chromatography (Figure 1A). In SDS-PAGE, a molecular mass of approximately 57 kDa was observed (Figure 1A), suggesting substantial glycosylation of the protein. Removal of the glycans with PNGaseF yielded a protein with an apparent molecular mass of 48 kDa (Figure 1B) corresponding to the expected molecular mass of the polypeptide chain. Under non-reducing conditions the band of ifnar1 was shifted to a lower molecular mass compared to the reduced protein, indicating internal disulfide bridge formation (Figure 1B). Glycosylated ifnar1-EC proved to be a stable protein, which was stored frozen at −80 °C. After one cycle of freezing and thawing, only insignificant loss of monomeric protein was observed by size-exclusion chromatography (Figure 1C). For all the following binding experiments, the glycosylated protein was used, because it was more stable than the deglycosylated protein.

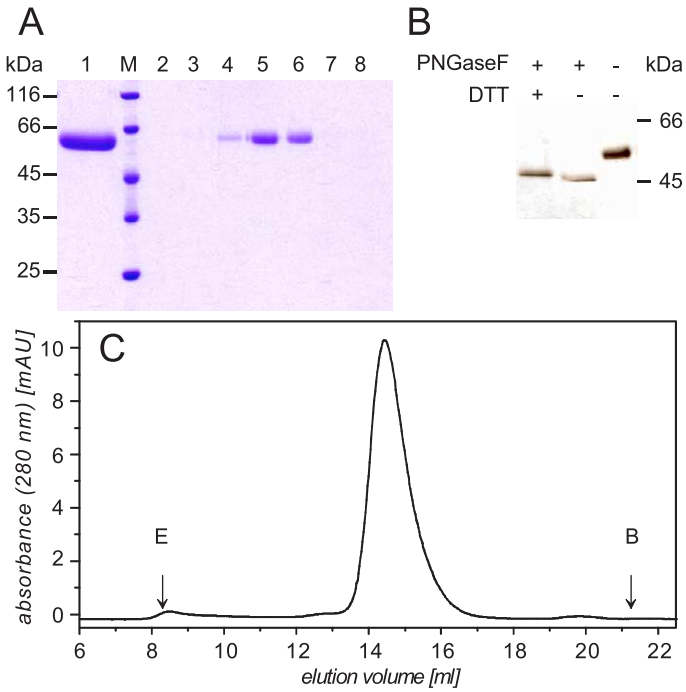

Figure 1. Purification and biochemical characterization of ifnar1-EC. A, SDS-PAGE of the purified protein: elution fraction from IMAC (lane 1) and fractions from size-exclusion chromatography (lane 2–8). B, SDS-PAGE of purified ifnar1-EC after deglycosylation with PNGaseF under non-reducing and reducing conditions in comparison to the non-deglycosylated protein. C, Size-exclusion chromatogram (Superdex 200 HR10/30) of purified ifnar1-EC after freezing and thawing (E, exclusion volume; B, bed volume).

We first characterized the interaction of ligands (IFNα2 and IFNβ with each of the receptor components (ifnar1-EC and ifnar2-EC) separately, in order to precisely determine affinities, rate constants and stoichiometries. These measurements were carried out by immobilizing either ifnar1-EC or ifnar2-EC *via* their C-terminal His-tag on the planar surface of the PEG polymer brush in an oriented fashion using high-affinity chelator head groups. Under these conditions, lateral interactions between the surface-attached proteins are minimized due to the short, covalently bound PEG chains. Protein binding was monitored label-free by RIfS detection. All binding data obtained from these measurements are summarized in Table 1.

Interaction of IFNs with ifnar2-EC

Binding of IFNα2 to immobilized ifnar2-tl has been studied before on different surfaces.[31] IFNα2 interacted specifically with ifnar2-EC immobilized *via* its C-terminal His-tag (Figure 2A) and the stoichiometry as determined from the relative binding amplitudes was 1 : 1. From concentration-dependent binding curves, a k_d value of $0.010(\pm 0.002)\ s^{-1}$, a k_a of $3(\pm 1) \times 10^6\ M^{-1}\ s^{-1}$ and a K_D of $3(\pm 1)$ nM were determined. These values are in excellent agreement with the values obtained for ifnar2-tl immobilized *via* monoclonal antibodies.[31] The association phase was significantly biased by mass transport limitation as indicated by the systematic deviation from the model (Figure 2C). Also the dissociation phase deviated significantly from a single-exponential decay indicating rebinding (Figure 2C) in agreement with that reported.[31] The interaction of IFNβ with immobilized ifnar2-EC had been investigated only at increased ionic strength in order to overcome its otherwise strong non-specific binding to the surface.[13] At the PEG polymer brush surface used in this study, no significant non-specific binding of IFNβ was detectable at physiological ionic strength after fully blocking the chelator head groups with MBP-H10 (Figure 2A). Under these conditions, IFNβ bound substantially tighter to ifnar2-EC compared to IFNα2 (Figure 2A), while from the relative signals, a 1 : 1 stoichiometry between ifnar2-EC and IFNβ was confirmed. The dissociation was very slow with an estimated k_d value of $0.0005\ s^{-1}$. From the I47A mutant of ifnar2-EC, IFNβ dissociated with a rate constant of $0.005(\pm 0.002)\ s^{-1}$ (Figure 2B). From this value, the k_d of approximately $0.0005\ s^{-1}$ was confirmed for the wild-type complex, assuming the same ten-fold difference as observed at high ionic strength.[13] Thus, the half-life of the complex with ifnar2-EC is probably about 20-fold higher for IFNβ compared to IFNα2. The observed association was strongly mass transport limited (Figure 2D), indicating that the association rate constant, k_a, is well above $5 \times 10^6\ M^{-1}\ s^{-1}$. The high k_a value can be explained by electrostatic rate enhancement, as IFNβ is positively charged and ifnar2-EC is strongly negatively charged at physiological pH.

The strong dependence of the complex stability on the ionic strength suggests that electrostatic forces also stabilize the interaction of IFNβ with ifnar2-EC. This effect, however, could also be due to rebinding on the surface, which is dependent on the k_a, value and thus also on the ionic strength. We therefore investigated the contribution of rebinding by injecting ifnar2-tl at high concentration (10 μM) during the dissociation phase (Figure 2E and F). In both cases, a significant faster

Table 1. Rate and equilibrium constants of the interaction with ifnar1-EC and ifnar2-EC determined for different IFNs and different mutants

	Ifnar2-EC			Ifnar1-EC			Ifnar2-EC/Ifnar1-EC[a]		
IFN	k_a ($M^{-1}\,s^{-1}$)	k_d (s^{-1})	K_D (nM)	k_a ($M^{-1}\,s^{-1}$)	k_d (s^{-1})	K_D (nM)	k_a ($M^{-1}\,s^{-1}$)	k_d (s^{-1})	K_D (nM)
IFNα2 wt	$(3 \pm 1) \times 10^6$	0.012 ± 0.002	3 ± 1	–	>0.5	5000 ± 2000	$(3 \pm 1) \times 10^6$	~ 0.0001	~ 0.03
IFNα2 S136C[b]	$(3 \pm 1) \times 10^6$	0.013 ± 0.002	3 ± 1		>0.5	~ 5000	$(3 \pm 1) \times 10^6$	~ 0.0001	~ 0.03
IFNα2 wt[c]	n.b.	n.b.	n.b.	–	>0.5	4000 ± 2000	n.b.	n.b.	n.b.
IFNα2 wt[d]	$(3 \pm 1) \times 10^6$	0.20 ± 0.04	60 ± 20	–	–	–	–	0.0012 ± 0.0002	–
IFNα2 R149A	–	~ 2	500 ± 100	–	>0.5	5000 ± 2000	–	0.010 ± 0.003	–
IFNβ	$>5 \times 10^6$	~ 0.001	<0.1	$(3 \pm 2) \times 10^5$	0.017 ± 0.004	50 ± 30	–	<0.0005	–
IFNβ[c]	n.b.	n.b.	n.b.	$(4 \pm 2) \times 10^5$	0.019 ± 0.004	50 ± 30	n.b.	n.b.	n.b.
IFNβ[e]	$>5 \times 10^6$	0.003 ± 0.001	<0.6	–	–	–	–	–	–
IFNβ[d]	$>5 \times 10^6$	0.005 ± 0.002	<1	–	–	–	–	<0.0005	–

Mean values and standard deviations were determined from at least three independent experiments. n.b., no binding detectable.

[a] Co-immobilized on lipid bilayers at high surface concentration.

[b] Labeled with OG-488 or AF-488 at the additional cysteine residue.

[c] In stoichiometric complex with ifnar2-tl.

[d] With the mutant ifnar2-EC I47A.

[e] At 500 mM NaCl.

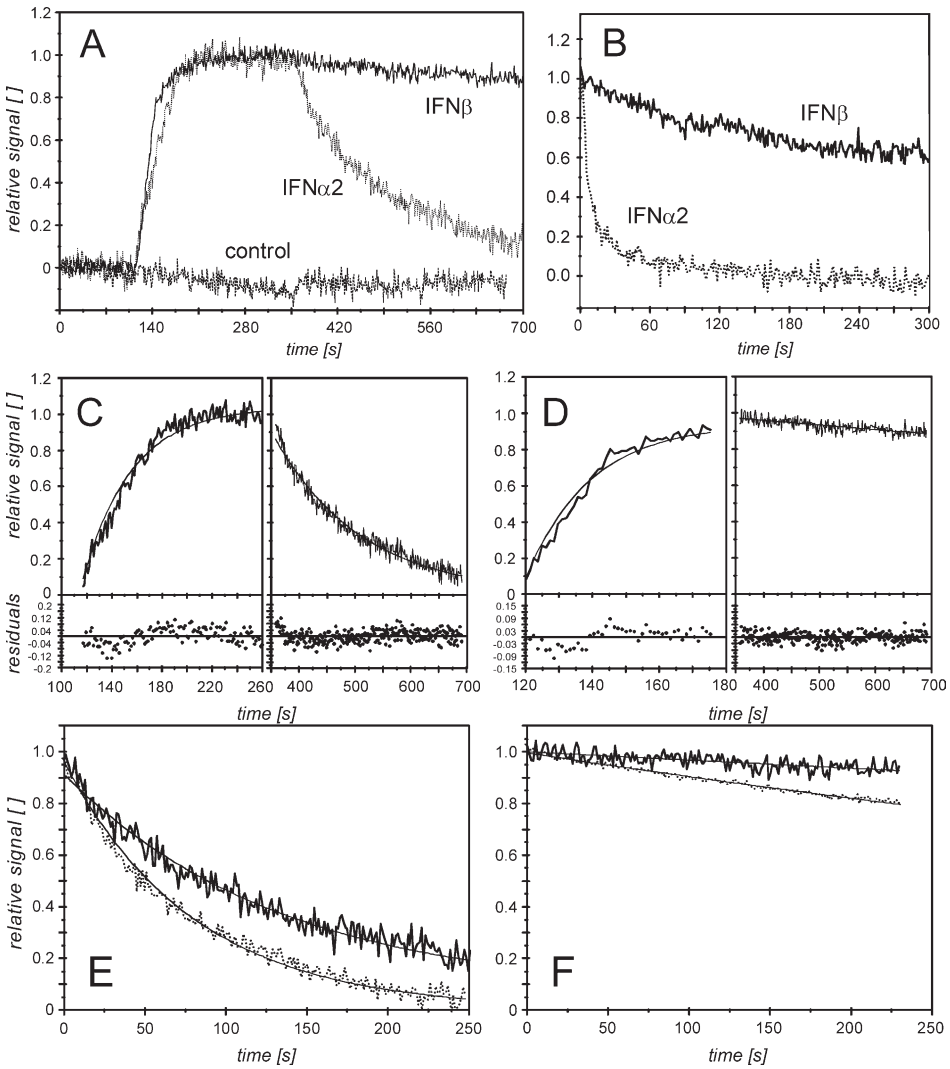

Figure 2. Interaction of IFNα2 and IFNβ with ifnar2-EC on a PEG polymer brush. A, Binding curve for 50 nM IFNα2 (·····) and 50 nM IFNβ (—) to ifnar2-EC in comparison to 50 nM IFNβ exposed to immobilized MBP-H10 (- - - -). B, Dissociation of IFNα2 (·····) and IFNβ (—) from immobilized ifnar2-EC I47A. C, Fit and residuals for association and dissociation of IFNα2 shown in A. D, Fit and residuals for association and dissociation of IFNβ shown in A. E and F, dissociation of IFNα2 (E) and IFNβ (F) from immobilized ifnar2-EC in the absence (—) and in the presence (·····) of 10 μM ifnar2-tl.

dissociation was observed resulting in corrected dissociation rate constants of 0.012(±0.003) s^{-1} for IFNα2 and ~0.001 s^{-1} for IFNβ, respectively.

Interaction of IFNs with ifnar1-EC

Binding of IFNα2 to immobilized ifnar1-EC was only detectable at concentrations above 300 nM and rapid dissociation was observed (Figure 3A). This interaction was entirely specific as confirmed by control experiments without ifnar1-EC on the surface (data not shown). From the equilibrium responses, R_{eq}, observed for IFNα2 at concentrations between 100 nM and 100 μM, titration curves were obtained (Figure 3B). A K_D value of 5(±2) μM was determined by fitting a Langmuir isotherm. Hence, the affinity of IFNα2 towards ifnar1-EC is about three orders of magnitude lower than for ifnar2-EC. The maximum binding signal, R_{max}, obtained from such titration corresponded to a 1 : 1 interaction between ifnar1-EC and IFNα2 assuming full activity of the immobilized ifnar1-EC. The same experiment was carried out with a stoichiometric complex of IFNα2 with ifnar2-tl. This complex with a life-time of ~100 s can be assumed static during the time-scale of the interaction with ifnar1-EC. Binding curves for the 0.1 μM and 10 μM IFNα2–ifnar2-tl complex are shown in Figure 3E. The relative binding signals obtained from a full titration (results not shown) confirmed a 1 : 1 stoichiometric ratio between the IFNα2–ifnar2-tl complex and immobilized ifnar1-EC. A K_D value of 4(±2) μM was obtained, which was not significantly different from the K_D determined for IFNα2 alone. This result suggests that the ternary complex of ifnar1, ifnar2 and IFNα2 is

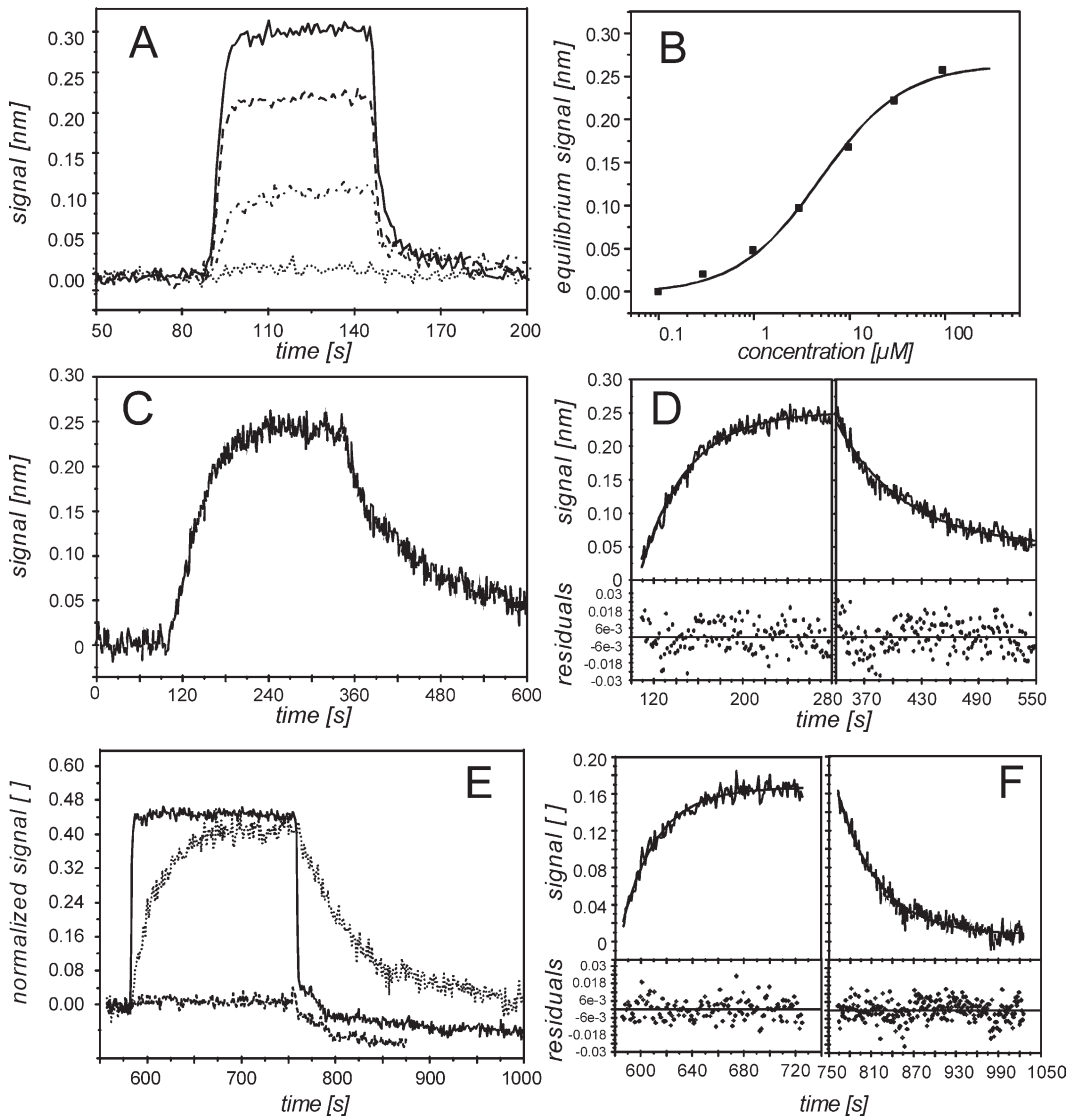

Figure 3. Binding of IFNs to immobilized ifnar1-EC on a PEG polymer brush. A, Binding of IFNα2 in various concentrations (100 nM, ·····; 1 μM, –·–·–, 10 μM, – – – –; 100 μM, —) to immobilized ifnar1-EC. B, Equilibrium response of IFNα2 binding to ifnar1-EC *versus* concentration and the fitted Langmuir isotherm. C, Binding of 50 nM IFNβ to immobilized ifnar1-EC. D, Monoexponential fit to the association and dissociation shown in C. E, Binding of 100 nM IFNβ–ifnar2-tl, 100 nM IFNα2–ifnar2-tl and 10 μM IFNα2–ifnar2-tl to immobilized ifnar1-EC in comparison (normalized to the amount of ifnar1-EC on the surface). F, Fit of single exponential models to the association and dissociation phase for the interaction of 100 nM IFNβ–ifnar2-tl with ifnar1-EC as shown in E, and the residuals of the fit.

not stabilized by additional interactions between ifnar1-EC and ifnar2-EC.

The interaction of IFNβ with immobilized ifnar1-EC was much more stable compared to the binding of the IFNα2 (Figure 3C). Association and dissociation phases were well fitted by monoexponential models (Figure 3D). From the fitting, a k_a value of $3(\pm 2) \times 10^5\ M^{-1}\ s^{-1}$ and a k_d value of $0.017(\pm 0.004)\ s^{-1}$ were obtained. The binding signals corresponded to a 1 : 1 stoichiometry between IFNβ and ifnar1-EC. Similar to IFNα2, no significant differences in the binding rates were observed for ifnar2-tl-bound IFNβ compared to free IFNβ (Figure 3E and F). Also a 1 : 1 stoichiometric ratio was confirmed. For free as well as ifnar2-tl-bound IFNβ a K_D value of 50(±30) nM was obtained. The interaction of the IFNβ–ifnar2-tl complex with ifnar1-EC was also investigated in solution by a binding inhibition assay (data not shown). The K_D value obtained from this experiment was 30(±10) nM, i.e. in good agreement with the K_D value determined for the interaction at the surface. Thus, the affinity of ifnar1-EC for IFNβ is two orders of magnitude higher than for IFNα2. Intriguingly, the association rate constant of IFNβ binding to ifnar1-EC is at least an order of magnitude lower compared to the binding to ifnar2-EC.

Complex formation on lipid bilayers

In order to analyze how the ternary complex is stabilized by lateral interaction on the membrane we investigated ternary complex formation on

solid-supported membranes. We tethered ifnar1-EC and ifnar2-EC to the surface of a solid-supported fluid lipid bilayer doped with chelator lipids using their C-terminal histidine-tags. When ifnar1-EC or ifnar2-EC were individually immobilized on solid-supported lipid bilayers, the binding curves obtained for IFNα2 and IFNβ binding to ifnar2-EC (Figure 4A and B) and ifnar1-EC (Figure 4C and D), respectively, were very similar to the corresponding measurements on the non-fluid polymer brush support. The rate and equilibrium constants obtained from these curves matched the rate constants determined from the measurements on non-fluid support. Neither for IFNα2 nor for IFNβ was significant non-specific binding detectable on the solid-supported lipid bilayers (Figure 4A, C and D).

Upon co-immobilization of ifnar1-EC and ifnar2-EC the binding kinetics of IFNα2 drastically changed (Figure 5A and B). No significant dissociation was observed within 15 minutes, and a second injection of IFNα2 did not give any significant signal (data not shown). Also the association kinetics was changed (Figure 5C–E): a constant binding rate until saturation was observed indicating highly diffusion-controlled binding. No dissociation of IFNα2 was discernible only if a 1 : 1 molar ratio for ifnar1-EC and ifnar2-EC was strictly maintained. With a molar excess of ifnar1-EC, we observed partial fast dissociation of IFNα2, and the amount of stably bound ligand corresponded to the amount of tethered ifnar2-EC (data not shown). With a molar excess of ifnar2-EC, we observed partial dissociation with a rate constant corresponding to the ifnar2–IFNα2 interaction, and the amount of stably bound ligand corresponded to the amount of ifnar1-EC on the bilayer (results not shown). These results confirmed that with IFNα2 a complex with a stoichiometry of 1 : 1 : 1 (or multiples thereof) was formed. Formation of a stable stoichiometric ternary complex was observed only on fluid supports (Figure 5B), confirming that orientation and lateral reorganization of the receptor domains were required to obtain maximum binding affinity. In order to characterize the lateral distribution of the immobilized proteins, laser scanning confocal fluorescence microscopy was carried out using ifnar2-EC-S35C labeled with OG-488 as a probe. Homogeneous lateral distribution of ifnar2-EC was observed on both polymer brush and supported membrane. The lateral diffusion of the receptor was investigated by FRAP experiments (Figure 6). No FRAP was observed for the polymer brush support (data not shown), while full FRAP was observed for the supported lipid bilayers (Figure 6A and B). For ifnar2-EC tethered to the chelator lipid, a diffusion constant of $1(\pm 0.5)\ \mu m^2/s$ was determined, which is very similar to the diffusion constant of GPI-anchored proteins in living cells.[32] No

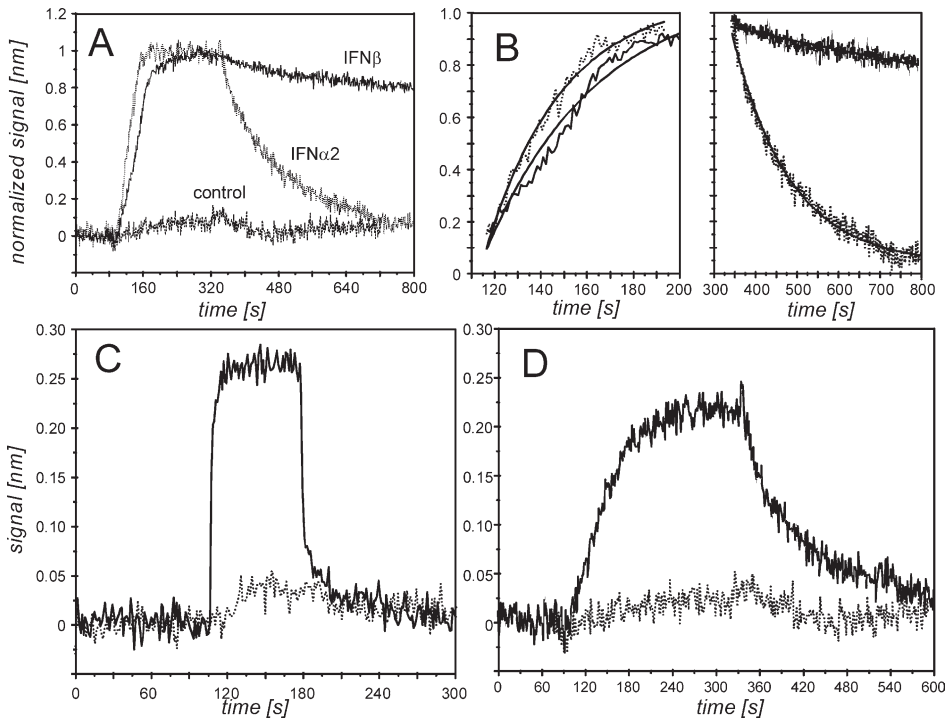

Figure 4. Ligand binding to ifnar1-EC and ifnar2-EC tethered on solid-supported lipid bilayers as detected by RIfS. A, Interaction of 50 nM IFNα2 (·····) and 50 nM IFNβ (—) with ifnar2-EC in comparison to 50 nM IFNβ exposed to a surface loaded with MBP-H10 (- - - -). B, Fit of the association and dissociation curves shown in A. C, Interaction of 10 μM IFNα2 (—) with immobilized ifnar1-EC in comparison to 10 μM IFNα2 exposed to a surface loaded with MBP-H10 (·····). D, Interaction of 100 nM IFNβ (—) with ifnar1-EC in comparison to 100 nM IFNβ exposed to a surface loaded with MBP-H10 (·····).

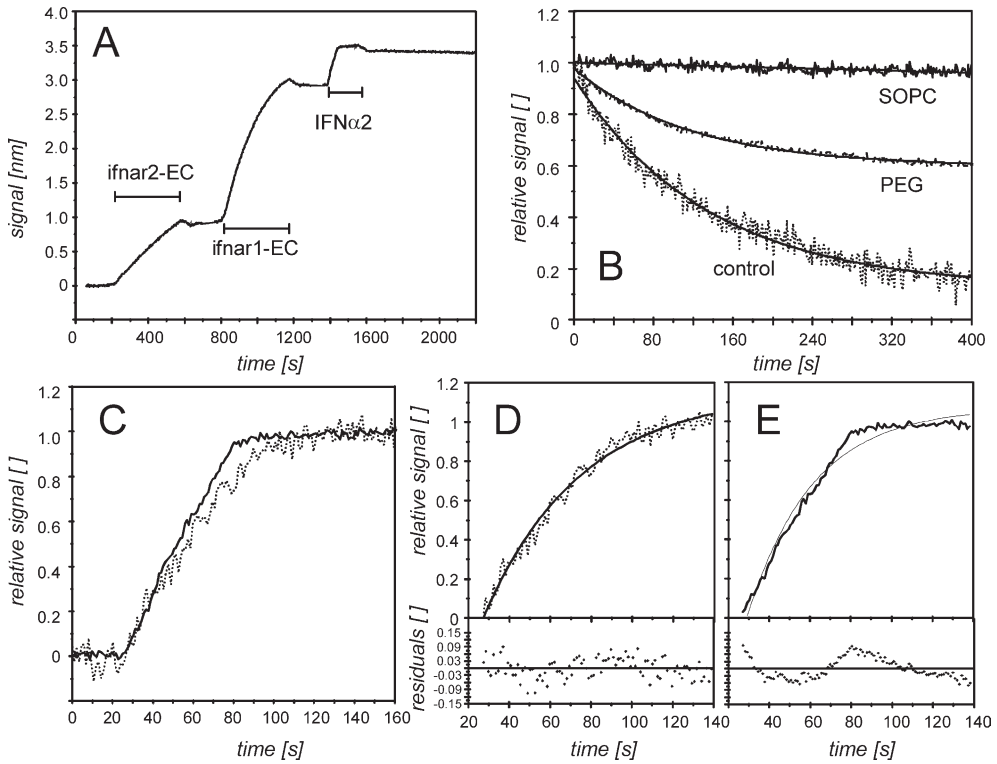

Figure 5. Ligand binding to ifnar1-EC and ifnar2-EC co-immobilized on solid-supported, fluid lipid bilayers. A, Immobilization of ifnar2-EC and ifnar1-EC in stoichiometric ratio, and interaction with 50 nM IFNα2. B, Dissociation of IFNα2 from the ternary complex with ifnar1-EC and ifnar2-EC on lipid bilayers (—) and on polymer brush support (- - - -), compared to the dissociation from ifnar2-EC alone (·····). C, Comparison of the association phases for binding of 50 nM IFNα2 to ifnar1-EC and ifnar2-EC on supported bilayers (—) and to ifnar2-EC alone (·····). D and E, Mono-exponential fit and residuals of the associations phases shown in C (with the same coding of the curves).

significant change in recovery time was observed upon co-immobilization with ifnar1, while binding of IFNα2 clearly reduced the recovery rate by a factor of 2 (Figure 6C). These results also confirmed that no substantial interaction between ifnar1-EC and ifnar2-EC takes place in the absence of the ligand.

Since for the wt proteins no dissociation from the ternary complex was observed, we investigated several mutants of ifnar2-EC and IFNα2 forming relatively less stable binary complexes with each other compared to their wild-type counterparts (Figure 7A and B). IFNα2 dissociates from ifnar2-EC I47A with a rate constant of 0.2 s^{-1} (20-fold higher than wt ifnar2-EC). Upon co-immobilization of ifnar-1EC, a k_d value of 0.0012(±0.0002) s^{-1} was observed (Figure 7C). For IFNα2 R149A (K_D, 500 nM, $k_d \approx 2\ s^{-1}$), a dissociation rate constant of 0.01(±0.003) s^{-1} in the presence of tethered ifnar1-EC was observed (Figure 7D). From these experiments it was estimated that in the presence of ifnar1-EC the apparent affinity is approximately 200-fold higher compared to the affinity towards ifnar2-EC alone.

All these measurements, however, were carried out at very high receptor surface concentrations (approximately 20–40 fmol/mm^2, i.e. 20–40% of a monolayer). The stability of the ternary complex at lower receptor concentration was studied using TIRFS because of the higher sensitivity of fluorescence detection compared to RIfS. Binding of fluorescent IFNα2 (S136C labeled with AF-488) to the receptor on lipid bilayers was measured at different surface concentrations of the receptor (Figure 8). At a high surface concentration of ifnar1-EC and ifnar2-EC, fluorescence detection principally showed similar dissociation phase as did RIfS (Figure 8A). However, a decay of the signal while rinsing was observed. This was not due to ligand dissociation, as stable binding was confirmed by simultaneous RIfS detection (data not shown), but can be ascribed to photobleaching. With a decreasing surface concentration of ifnar1-EC and ifnar2-EC we observed a decreasing stability of the ternary complex (Figure 8B). The dissociation curves were fitted by a single-exponential decay (Figure 8B and C), and increasing k_d values were obtained with decreasing surface concentrations. In Figure 8D, the dissociation rate constants were plotted as a function of receptor surface concentration, the corresponding values are listed in Table 2. At the lowest receptor surface concentration of approximately 0.3 fmol/mm^2 (~200 molecules/μm^2), the stability of the ternary complex was only three times higher than for ifnar2-EC alone. For surface concentrations of 2–4 fmol/mm^2 we determined k_d values corresponding to the affinities that have been

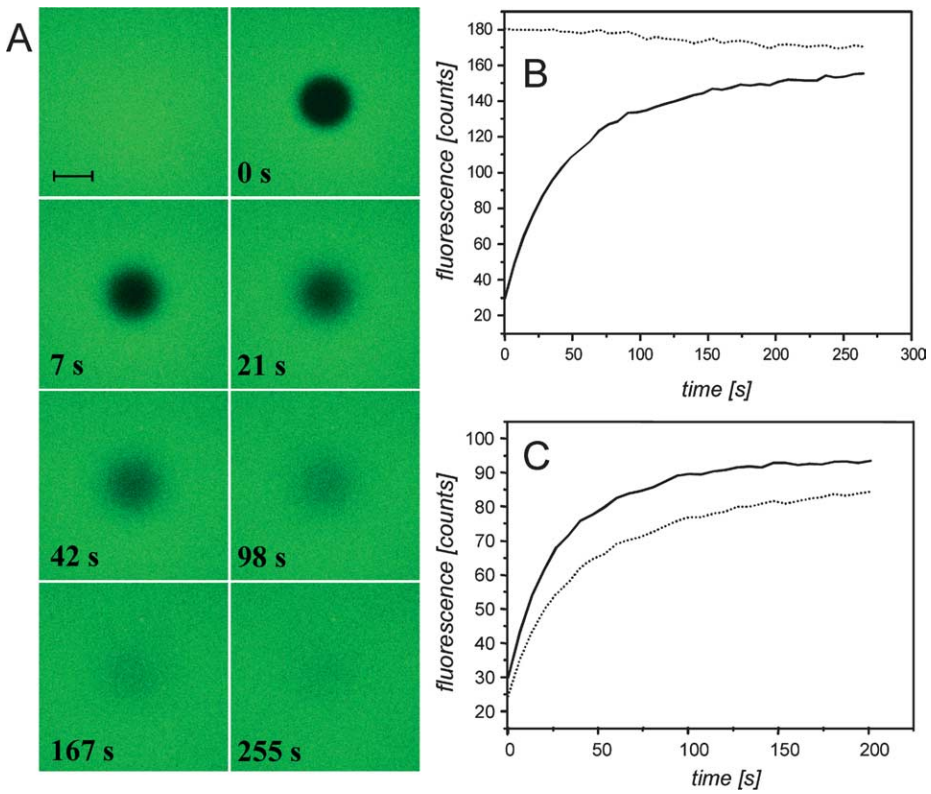

Figure 6. FRAP experiment with ifnar2-EC S35C labeled with OG488 tethered to chelator lipids in a solid-supported lipid bilayer. A, Fluorescence images of ifnar2-EC OG-488 tethered to a solid-supported lipid bilayer before and after bleaching of a circular spot (the time after bleaching is indicated in the lower left corner of each image, the bar represents 20 μm). B, Fluorescence intensity in the bleached spot as a function of time (—) compared to a non-bleached reference spot (·····). C, Recovery curves of ifnar2-EC OG-488 in the presence of ifnar1-EC before (—) and after (·····) addition of 100 nM IFNα2.

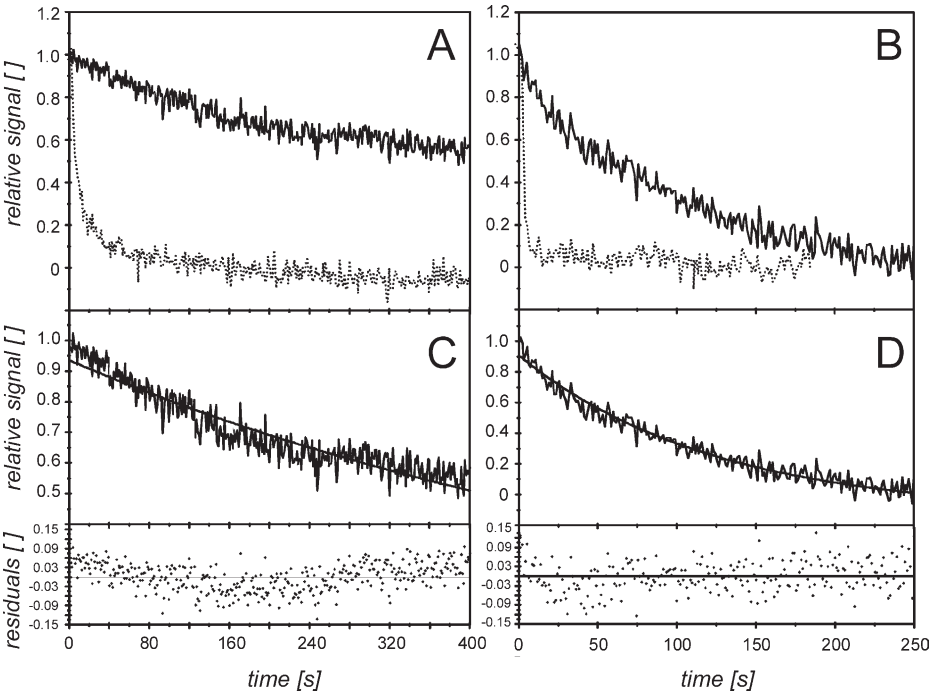

Figure 7. Dissociation of IFNα2 from both ifnar1-EC and ifnar2-EC on lipid bilayers (—) compared to ifnar2-EC alone (·····) observed for ifnar2-EC I47A with wild-type IFNα2 (A) and for wild-type ifnar2-EC with IFNα2 R149A (B). C and D, Fit of a mono-exponential decay to the dissociation from the ternary complex shown in A (C) and B (D), and the residuals.

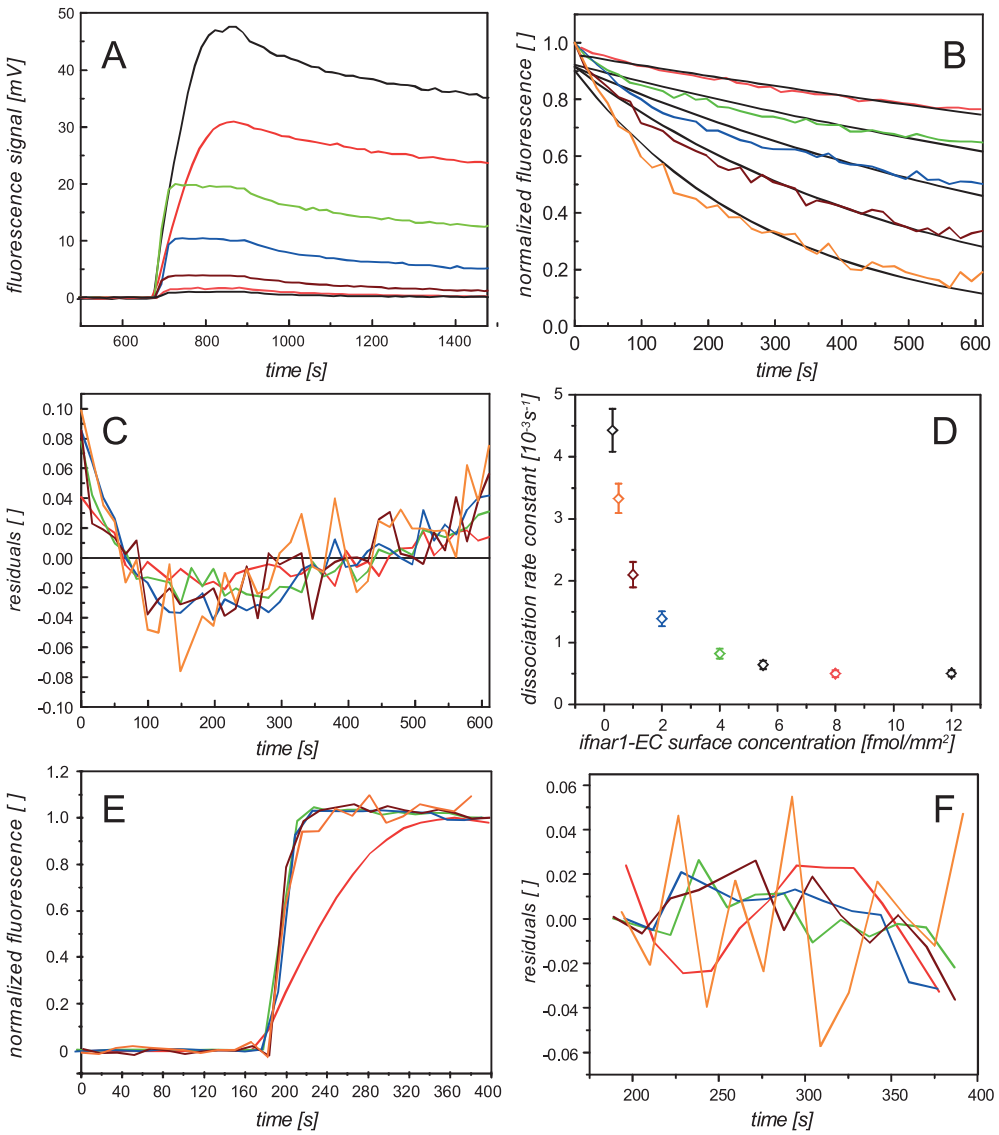

Figure 8. The IFNα2 interaction with ifnar1-EC and ifnar2-EC tethered onto supported lipid bilayers as detected by TIRFS. A, Binding of 100 nM AF-488-labeled IFNα2 at different surface concentrations of ifnar2-EC and ifnar1-EC in a stoichiometric ratio (black, 12 fmol/mm^2; red, 8 fmol/mm^2; green, 4 fmol/mm^2; blue, 2 fmol/mm^2; brown, 1 fmol/mm^2; orange, 0.5 fmol/mm^2). B, Dissociation phases of the binding curves shown in A normalized to the signal at the beginning of dissociation (same color coding as for A) including the fit curve of a mono-exponential decay (black lines). C, Residuals for fitting curves shown in B (same color coding as for A). D, Dissociation rate constant as a function of the surface concentration of the receptor. E, Association phases of binding curves shown in A normalized to the saturation signal (same color coding as for A). F, Residuals of a first-order association model fitted to the curves shown in E.

observed in binding assays with living cells.[33] The association phases of the binding curves normalized to the saturation signal are shown in Figure 8E. At receptor surface concentrations below 8 fmol/mm^2, the association curves overlayed. These curves were fitted well by a pseudo-first-order model (Figure 8F) and gave association rate constants very similar to the interaction of IFNα2 with ifnar2-EC alone (Table 2). At a higher surface concentration, significant lower association rate constants were obtained and systematic deviations from the model, as well as from the other binding curves were observed (Figure 8F). This was probably due to mass transport limitations at these high receptor surface concentrations, which have already been observed for the interaction of IFNα2 with ifnar2-EC alone.

The dependence of the complex stability on the receptor surface concentration suggested that the ternary complex is not static, but stabilized by fast re-association, the kinetics of which depends on the receptor surface concentration. This was further corroborated by the observation that stable ternary complexes were formed at low surface concentrations of ifnar2-EC but high surface concentrations of ifnar1-EC (results not shown). In

Table 2. Rate and equilibrium constants of IFNα2 binding at different stoichiometric surface concentrations of ifnar1-EC and ifnar2-EC on supported lipid bilayers

Ifnar1-EC (fmol/mm^2)	k_a (10^6 M^{-1} s^{-1})	k_d (10^{-3} s^{-1})	K_D (nM)[a]
12 ± 3	1 ± 0.3	0.5 ± 0.1	0.17 ± 0.06
8 ± 2	1 ± 0.3	0.5 ± 0.1	0.17 ± 0.06
5.5 ± 1	3 ± 1	0.6 ± 0.1	0.21 ± 0.07
4 ± 1	4 ± 1	0.8 ± 0.2	0.28 ± 0.1
2 ± 0.4	5 ± 2	1.4 ± 0.2	0.46 ± 0.16
1 ± 0.2	3.5 ± 1	2.1 ± 0.2	0.70 ± 0.24
0.5 ± 0.1	3 ± 1	3.3 ± 0.3	1.11 ± 0.4
0.3 ± 0.1	4 ± 1	4.4 ± 0.4	1.48 ± 0.5
0	4 ± 1	12 ± 1	4 ± 1.5

[a] Calculated using the average k_a of $3(\pm 1) \times 10^6$ M^{-1} s^{-1}.

order to analyze this kinetic stabilization, we challenged the apparently stable ternary complex formed with fluorescently labeled IFNα2 (S136C with OG-488) by injecting unlabeled IFNα2 or ifnar2-tl (Figure 9A). Already at a concentration of 1 μM unlabeled IFNα2, an exchange rate of 0.002 s^{-1} was observed. At the same time the total amount of bound IFN did not change as simultaneously detected by RIfS (data not shown). In contrast, no significant change in dissociation kinetics was observed when ifnar2-tl was injected, even at a concentration as high as 10 μM (Figure 9A). Furthermore, even at much lower surface concentrations of ifnar2-EC (~0.5 fmol/mm^2), fast exchange was observed in the presence of 1 μM unlabeled IFNα2 (Figure 9B). These experiments confirm that the ligand does not dissociate from the surface and re-associates (rebinding-effect), because then ifnar2-tl should interfere as efficiently as does IFNα2, and the effect should be much less pronounced at low surface concentrations. The fact that the ligand is exchanged much faster than the apparent dissociation rate furthermore corroborates the kinetic stabilization of the ternary complex.

Binding assays with ifnar1 and ifnar2 co-immobilized on lipid bilayers were also carried out with IFNβ. However, very stable binding was observed already for the interaction with ifnar2-EC alone, and thus no substantial difference in stability could be observed in the presence of ifnar1-EC. Upon challenging the ternary complex formed with IFNβ by injecting fluorescently labeled IFNα2, no exchange could be observed (data not shown), confirming the anticipated high stability of the ternary complex. Since the already formulated IFNβ could not be labeled appropriately, binding assays at low surface concentration were also not feasible.

Discussion

In this study we dissected the individual contributions of the different interactions between ifnar1-EC, ifnar2-EC and IFNs involved in formation of the ternary complex. For understanding their role for ligand-induced receptor assembling, we investigated the ternary complex formation by tethering the extracellular receptor domains in an oriented fashion on supported membranes. Based on combined fluorescence and label-free detection we studied receptor assembling on a mechanistic level, which may help to explain how differences in receptor engagement by IFNα2 and IFNβ result in differential signaling.

Interaction between ifnar1 and ifnar2

Interaction between receptor components cross-linked by binding to different sites of a ligand is the basic paradigm for cytokine receptor activation. Yet the mode of its induction is currently under controversial debate, and probably different modes apply for different systems.[34,35] Increasingly, pre-association of the receptor chains,[27,29,36] and their activation by ligand-induced conformational

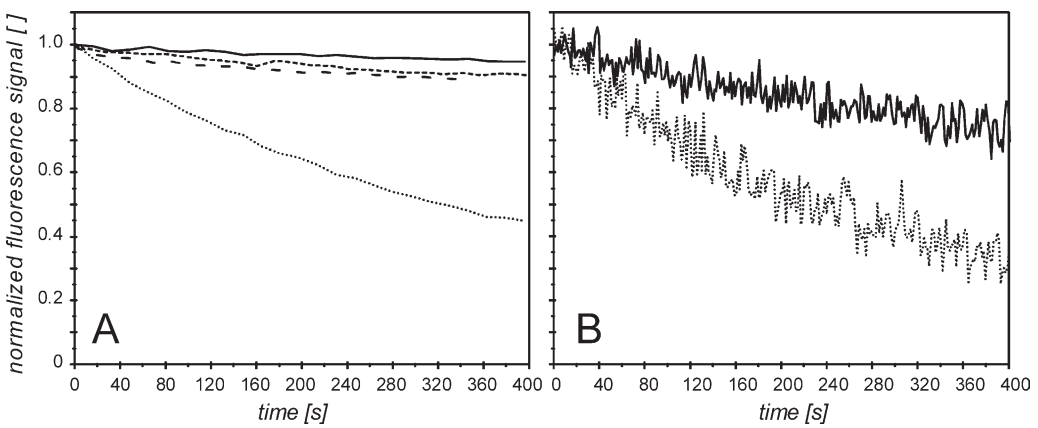

Figure 9. Chase experiments with fluorescent-labeled IFNα2 bound to ifnar2-EC and ifnar1-EC co-immobilized on supported lipid bilayers. A, Dissociation of OG-488-labeled IFNα2 (—) at high surface concentrations of both ifnar2-EC and ifnar1-EC, in the presence of 1 μM (- - - -) and 10 μM (– – – –) ifnar2-tl, and in the presence of 1 μM unlabeled IFN (·····). B, Dissociation of OG-488-labeled IFNα2 from the ternary complex at low surface concentration of ifnar2-EC in the absence (—) and in the presence (·····) of 1 μM unlabeled IFNα2.

changes have been postulated. In the case of class I cytokine receptors, namely growth hormone receptor,[37,26] interleukin-4 receptor[23] and interleukin-6 receptor,[24] stem–stem contacts between the membrane-proximal, extracellular receptor domains have been shown to be important for the formation of stable ternary complexes. Though the affinities of such receptor–receptor interactions have not been quantified yet, stabilization by cooperative inter-receptor and ligand-receptor contacts was clearly shown. Gel-filtration assays carried out with recombinant ifnar1-EC, ifnar2-EC and IFNβ indicated a similar scenario for the type I interferon receptor.[21] For both IFNα2 and IFNβ, we could clearly exclude such co-operative interaction, as we did not detect a significant difference in the affinity of ifnar1-EC for free compared to ifnar2-tl-complexed ligand. Furthermore, no direct interaction between ifnar1-EC and ifnar2-EC was detectable, neither by solid-phase detection nor by FRAP. These results suggest a different mode of interaction for this member of the class II cytokine receptor superfamily compared to the members of the class I family mentioned above. This is in good agreement with the observation that the binding site for IFNα is not located on the membrane-proximal tandem Ig-like domains, but at the hinge between the two extracellular tandem Ig-like domains of ifnar1-EC.[18,20]

Kinetic stabilization of the ternary complex with IFNα2

In order to understand the contributions of the individual interactions towards the stability of the ternary complex on the cell surface, we studied complex formation with ifnar1-EC and ifnar2-EC tethered onto solid-supported membranes. IFNα2 binding was extremely stable at high surface concentrations of ifnar1-EC and ifnar2-EC, decreasing the apparent k_d value compared to ifnar2-EC alone by approximately 200-fold. The dependence of the complex stability on the surface concentration of the receptor and the possibility of exchanging the bound ligand with much faster rates than the apparent dissociation rate constant suggest kinetic rather than static stabilization of the complex. The k_d value of $>0.5\,s^{-1}$ for the interaction between ifnar1-EC and the IFNα2–ifnar2-tl complex implies that the life-time of an individual ternary complex is of the order of a second. Since we could not observe direct interactions between ifnar2-EC and ifnar1-EC, we propose a two-step assembling mechanism as shown in Figure 10 after binding of IFNα2 to ifnar2 (k_1), ifnar1 transiently associates in a second step to the complex. Owing to the short life-time of the IFNα2–ifnar1 interaction, the complex dissociates (k_{-2}) and re-associates (k_2) in a fast manner (on a sub-second scale). Thus, depending on the receptor surface concentrations, only part of the bound ligand is involved in the ternary complex. This fraction is defined by the equilibrium dissociation constant for the interaction of the ifnar2-EC–IFN complex with ifnar1-EC on the surface $K_2 = k_{-2}/k_2$. Since direct dissociation of IFNα2 from the ternary complex is very unlikely (at least 200-fold slower than from ifnar2-EC alone), the apparent k_d value reflects the fraction of ifnar2-EC–IFNα2 not in complex with ifnar1-EC. In cellular binding assays, a 10–40-fold decrease in K_D caused by ifnar1 has been observed for IFNα2.[33] Assuming that the biophysical environment is in principle mimicked appropriately, our results have several important implications for the mechanism of receptor assembling. (i) The formation of a stable pre-formed receptor-complex by interactions mediated *via* the extracellular domains as suggested for other receptors[25,27,28] is very unlikely. (ii) The receptor components are in some way co-localized on the surface of the plasma membrane, as random distribution of several hundred receptors on the plasma membrane would not be sufficient for gaining 20–40 times increased stability. This is in line with the observation that ifnar1 and ifnar2 are located in caveolae,[38] leading to a higher effective concentration. (iii) Different receptor concentrations not only lead to different apparent binding affinities, but also different fractions of IFN involved in the ternary complex. This could explain the different actions and relative activities of IFNs on different cell types.

Differential signaling

One striking observation of this study was the much higher affinity of IFNβ compared to IFNα2 not only towards ifnar2-EC, but even more dramatically towards ifnar1-EC. This result is consistent with the observation that ifnar1 co-immunoprecipitated with ifnar2 in presence of IFNβ, but

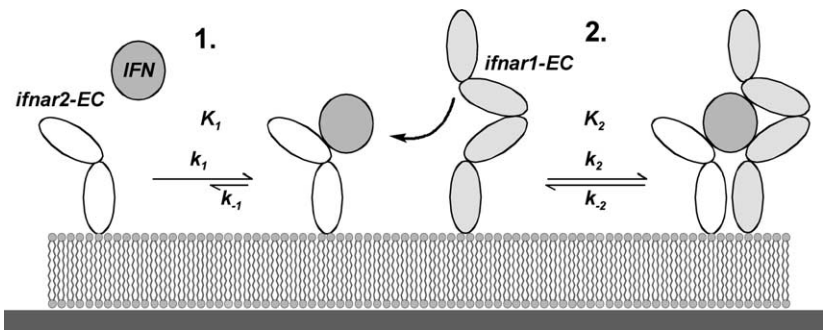

Figure 10. Scheme of a two-step formation and kinetic stabilization of the ternary complex upon IFN binding.

not IFNα2.[5,8] The higher affinity of ifnar1-EC towards ifnar2-EC and ifnar1-EC has two main consequences: first of all it implies that IFNβ binds to the cellular receptor with more than one order of magnitude higher affinity than IFNα2. For IFNα2 mutants, a clear correlation between affinity towards ifnar2-EC and anti-viral activity has been shown.[14] The antiviral activity of IFNβ is only by a factor of 2 to 4 higher than for IFNα2, and not by orders of magnitude. However, saturation of activity has also been observed for human growth hormone upon enhancing its binding affinity substantially.[39] While the reason for this saturation is not fully clear, it is plausible, that this effect is different for different types of responses. Second, the higher affinity of IFNβ towards ifnar1 implies more efficient ternary complex formation at low receptor surface concentrations and longer stability of individual ternary complexes compared to IFNα2. Such differential efficiencies in the engagement of ifnar1 (and ifnar2) by IFNβ compared to IFNα2 could then explain several features of differential signal activation by IFNs: (i) compared to IFNα, IFNβ shows additional gene activation at lower (i.e. physiological) concentrations, while at higher concentration similar activities were observed;[11] (ii) differential signaling is dependent on the cell type,[9] which may be related to (local) receptor concentrations. Further studies, and in particular binding experiments with full transmembrane proteins in living cells, will be required to test this hypothesis fully. Strikingly, the important role of the surface affinity K_2 (cf. Figure 10) for the formation of the IL4 receptor complex has been demonstrated in living cells.[40]

Materials and Methods

Materials

IFNβ (formulated Rebif 22 μg and 44 μg) was a gift from Serono GmbH, Unterschleißheim, Germany. Oregon green 488 (OG-488) maleimide and Alexa Fluor 488 (AF-488) maleimide were purchased from Molecular Probes Europe BV, Leiden, Netherlands. Synthetic stearoyl-oleoyl phosphatidylcholine (SOPC) was purchased from Avanti Polar Lipids, Alabaster, USA. The vector pACgp67B and the BaculoGold baculovirus kit were purchased from BD Biosciences GmbH, Heidelberg, Germany. The vector pMAL-c2x and PNGaseF were purchased from New England Biolabs, Frankfurt am Main, Germany.

Protein expression, purification and labeling

IFNα2, IFNα2-R149A and tag-less ifnar2-EC (ifnar2-tl) were expressed in *Escherichia coli*, refolded from inclusion bodies and purified by anion-exchange and size-exclusion chromatography as described.[41] The wt ifnar2-EC carrying a C-terminal decahistidine-tag and its mutant I47A were expressed and purified in the same manner. The ifnar2-EC mutant S35C and the IFNα2 mutant S136C were refolded and purified as the wt. After size-exclusion chromatography, the proteins were labeled by adding a threefold molar excess of OG-488 maleimide or AF-488 maleimide at 4 °C for 18 hours. Finally, they were further purified by desalting and anion-exchange chromatography. Binding experiments confirmed that the interaction properties of both proteins were not affected by mutagenesis and labeling. OG-488 and AF-488 labeled proteins showed very similar properties in terms of fluorescence intensities and bleaching rates. Ifnar1-EC with a C-terminal His-tag was cloned into the vector pACgp67B and expressed in *Sf9* insect cells using the baculovirus system (BaculoGold). The supernatant was harvested three to four days after infection and ifnar1-EC was purified by immobilized metal chelate affinity chromatography (IMAC) and size-exclusion chromatography. The protein was analytically deglycosylated using PNGaseF. MBP-H10 was expressed using the pMal-c2x vector and purified by IMAC and size-exclusion chromatography. All purified proteins were more than 95% homogeneous and monomeric as detected by non-reducing SDS-PAGE and size-exclusion chromatography.

Solid phase detection techniques

Receptor immobilization, lipid bilayer assembling and protein interactions were monitored by RIfS. This label-free detection technique monitors binding on the surface of a thin silica interference layer,[42,43] and therefore is compatible with fluorescence detection. Furthermore, background signals due to changes in the bulk refractive index as observed by evanescent field detection are much less critical in RIfS-detection.[31] Binding curves were obtained from the shift of the interference spectrum of the silica layer: a shift of 1 nm corresponds to approximately 1 ng/mm^2 protein on the surface. Measurements were carried out in a flow chamber with an acquisition rate of 1 Hz under continuous flow-through conditions as described.[31,42]

Binding of fluorescence-labeled proteins was monitored by TIRFS using a home-built setup. A 25 mW argon ion laser was used for fluorescence excitation at 488 nm. Typically a low excitation power of 2–3 μW focused onto an area of ~1–2 mm^2 was used in order to minimize photobleaching. Fluorescence was collected by an optical fiber and detected by a photomultiplier tube through a bandpass filter. The same transducer slides as for RIfS detection were used as substrates, and all processes on the surface were monitored simultaneously by single-wavelength RIfS detection at 800 nm. The combined TIRFS-RIfS set-up will be described in more detail elsewhere. Continuous flow-through conditions were maintained for all experiments. Data were acquired with a time resolution between 1.5 s and 16 s, depending on the kinetics of the process. Photobleaching was minimized by closing the shutter of the excitation source between the measurements.

Surface modification

For probing the interactions between individual proteins involved in the formation of the ternary complex, the silica surface of the transducer was modified with a two-dimensional molecular polymer brush of poly(ethylene glycol) (PEG) as described.[44] For oriented immobilization, a chelator head group carrying nitrilotriacetic acid (NTA) moieties was covalently coupled to the PEG polymer brush. This chelator head group binds decahistidine-tagged proteins with high stability

allowing complete blocking of excessive binding sites. Its synthesis and characterization will be described elsewhere.

Solid-supported lipid bilayers were obtained by vesicle fusion on the bare silica surface of the transducer as described.[45] SOPC in chloroform was mixed with 1–5 mol% of a chelator lipid based on the same chelator head group mentioned above. After removing the solvent *in vacuo* and resuspension into buffer, small unilaminar vesicles (SUV) were prepared by probe sonication. The transducer surface was incubated for 30 minutes in a freshly prepared mixture of two parts 30% (v/v) hydrogen peroxide and three parts concentrated sulfuric acid. After extensive washing with water, the transducer was mounted immediately into the flow cell. SUVs at a concentration of 250 μM were injected and bilayer formation was followed by RIfS-detection.

Binding assays

All binding assays were carried out in 20 mM Hepes (pH 7.5) and 150 mM NaCl. The chelator head groups were loaded with Ni ions by injecting 15 mM nickel(II)-chloride in running buffer. Depending on the targeted surface concentrations, the histidine-tagged receptor proteins were injected at concentrations between 2 nM and 1 μM for 100–400 s. Excessive binding sites were blocked by injecting 1 μM decahistidine-tagged maltose-binding protein (MBP-H10). Immobilized proteins were removed with a pulse of 200 mM imidazole (pH 8.0). Ligand binding experiments and their evaluation were carried out as described.[31] Protein solutions were diluted at least five-fold into the running buffer to avoid background signals. As a control for specificity, the highest protein concentration was applied either without immobilized protein or after immobilizing MBP-H10. Complex stoichiometries were estimated from the relative saturation signals taking the molecular masses of the proteins into account. In the case of rate constants below $0.3\ s^{-1}$, association and dissociation rate constants were determined by fitting a single-exponential function and assuming a 1 : 1 interaction stoichiometry. Low-affinity interactions with $k_d > 0.3\ s^{-1}$ were investigated by determining the equilibrium response at various ligand concentrations. The equilibrium dissociation constant K_D was determined from dose-response curves by fitting the Langmuir equation. For studying the interaction of complexes of IFNs and ifnar2-EC with immobilized ifnar1-EC, ifnar2-tl was added in stoichiometric amounts, and formation of the stoichiometric complex was verified by analytical gel-filtration.[41] The K_D value of the interaction of ifnar1-EC with IFNβ–ifnar2-EC complex in solution was determined by a binding inhibition assay with 20 nM IFNβ–ifnar2-EC and ifnar1-EC at concentrations between 10 nM and 1 μM. The initial slope *versus* ifnar1-EC concentration in solution was plotted and the K_D value determined by fitting the exact solution of the law of mass action as described.[46]

Fluorescence recovery after photo-bleaching (FRAP)

Fluorescence imaging and recovery experiments were carried out with a laser scanning confocal microscope (LSM 510; Zeiss, Jena) equipped with a 25 mW argon ion laser. Bilayer assembling and receptor attachment were carried out in a flow cell with automated sample handling. The ifnar2-EC mutant S35C labeled with OG-488 was immobilized as described above. A circular spot with a diameter of 20–30 μm was bleached by scanning for 9 s at 75% laser power. Immediately afterwards images were acquired at 0.1–0.4% laser power by scanning for 1.9 s with a time interval of 5–10 s. Diffusion constants were calculated from the $\tau_{1/2}$ determined from the recovery curves as described[47] using a γ-factor of 1.

Acknowledgements

IFNβ (Rebif) was provided by Dr H.-J. Obert, Serono GmbH, Unterschleißheim. The expression vectors for IFNα2 and ifnar2-EC were obtained from Gideon Schreiber, Weizmann Institute of Science. A vector containing the gene of ifnar1-EC was obtained from Gilles Uzé, CNRS Montpellier. Labeled IFNα2 was prepared by Pia Müller. We thank Bernd Otto, Fraunhofer IGB, Hannover for helpful discussions. This work was supported by the Deutsche Forschungsgemeinschaft within the Emmy-Noether Program for young investigators (PI-405/1-1,2), by the Human Frontier Science Program (RGP60/2002) and by Stiftung P.E: Kempkes (10/2000). The support from the laboratory of Robert Tampé is gratefully acknowledged, in particular the help of Eckhard Linker with insect cell culture.

References

1. Deonarain, R., Chan, D. C., Platanias, L. C. & Fish, E. N. (2002). Interferon-alpha/beta-receptor interactions: a complex story unfolding. *Curr. Pharm. Des.* **8**, 2131–2217.
2. Uze, G., Lutfalla, G. & Mogensen, K. E. (1995). Alpha and beta interferons and their receptor and their friends and relations. *J. Interferon Cytokine Res.* **15**, 3–26.
3. Abramovich, C., Shulman, L. M., Ratovitski, E., Harroch, S., Tovey, M., Eid, P. & Revel, M. (1994). Differential tyrosine phosphorylation of the IFNAR chain of the type I interferon receptor and of an associated surface protein in response to IFN-alpha and IFN-beta. *EMBO J.* **13**, 5871–5877.
4. Platanias, L. C., Uddin, S., Domanski, P. & Colamonici, O. R. (1996). Differences in interferon alpha and beta signaling. Interferon beta selectively induces the interaction of the alpha and betaL subunits of the type I interferon receptor. *J. Biol. Chem.* **271**, 23630–23633.
5. Croze, E., Russell-Harde, D., Wagner, T. C., Pu, H., Pfeffer, L. M. & Perez, H. D. (1996). The human type I interferon receptor. Identification of the interferon beta-specific receptor-associated phosphoprotein. *J. Biol. Chem.* **271**, 33165–33168.
6. Mintzer, R. J., Croze, E., Rubanyi, G. M. & Johns, A. (1998). Differential effects of IFN-beta1b on the proliferation of human vascular smooth muscle and endothelial cells. *J. Interferon Cytokine Res.* **18**, 939–945.
7. Domanski, P., Nadeau, O. W., Platanias, L. C., Fish, E., Kellum, M., Pitha, P. & Colamonici, O. R. (1998). Differential use of the betaL subunit of the type I interferon (IFN) receptor determines signalling

specificity for IFNalpha2 and IFNbeta. *J. Biol. Chem.* **273**, 3144–3147.
8. Russell-Harde, D., Wagner, T. C., Perez, H. D. & Croze, E. (1999). Formation of a uniquely stable type I interferon receptor complex by interferon beta is dependent upon particular interactions between interferon beta and its receptor and independent of tyrosine phosphorylation. *Biochem. Biophys. Res. Commun.* **255**, 539–544.
9. Grumbach, I. M., Fish, E. N., Uddin, S., Majchrzak, B., Colamonici, O. R., Figulla, H. R. *et al.* (1999). Activation of the Jak-Stat pathway in cells that exhibit selective sensitivity to the antiviral effects of IFN-beta compared with IFN- alpha. *J. Interferon Cytokine Res.* **19**, 797–801.
10. Der, S. D., Zhou, A., Williams, B. R. & Silverman, R. H. (1998). Identification of genes differentially regulated by interferon alpha, beta, or gamma using oligonucleotide arrays. *Proc. Natl Acad. Sci. USA*, **95**, 15623–15628.
11. da Silva, A. J., Brickelmaier, M., Majeau, G. R., Lukashin, A. V., Peyman, J., Whitty, A. & Hochman, P. S. (2002). Comparison of gene expression patterns induced by treatment of human umbilical vein endothelial cells with IFN-alpha 2b *versus* IFN-beta 1a: understanding the functional relationship between distinct type I interferons that act through a common receptor. *J. Interferon Cytokine Res.* **22**, 173–188.
12. Runkel, L., Pfeffer, L., Lewerenz, M., Monneron, D., Yang, C. H., Murti, A. *et al.* (1998). Differences in activity between alpha and beta type I interferons explored by mutational analysis. *J. Biol. Chem.* **273**, 8003–8008.
13. Piehler, J. & Schreiber, G. (1999). Mutational and structural analysis of the binding interface between type I interferons and their receptor ifnar2. *J. Mol. Biol.* **294**, 223–237.
14. Piehler, J., Roisman, L. C. & Schreiber, G. (2000). New structural and functional aspects of the type I interferon- receptor interaction revealed by comprehensive mutational analysis of the binding interface. *J. Biol. Chem.* **275**, 40425–40433.
15. Roisman, L. C., Piehler, J., Trosset, J. Y., Scheraga, H. A. & Schreiber, G. (2001). Structure of the interferon-receptor complex determined by distance constraints from double-mutant cycles and flexible docking. *Proc. Natl Acad. Sci. USA*, **98**, 13231–13236.
16. Chill, J. H., Quadt, S. R., Levy, R., Schreiber, G. & Anglister, J. (2003). The human type I interferon receptor. NMR structure reveals the molecular basis of ligand binding. *Structure (Camb)*, **11**, 791–802.
17. Runkel, L., De Dios, C., Karpusas, M., Baker, D., Li, Z., Zafari, M. *et al.* (2001). Mapping of IFN-beta epitopes important for receptor binding and biologic activation: comparison of results achieved using antibody- based methods and alanine substitution mutagenesis. *J. Interferon Cytokine Res.* **21**, 931–941.
18. Lu, J., Chuntharapai, A., Beck, J., Bass, S., Ow, A., De Vos, A. M. *et al.* (1998). Structure-function study of the extracellular domain of the human IFN-alpha receptor (hIFNAR1) using blocking monoclonal antibodies: the role of domains 1 and 2. *J. Immunol.* **160**, 1782–1788.
19. Goldman, L. A., Cutrone, E. C., Dang, A., Hao, X., Lim, J. K. & Langer, J. A. (1998). Mapping human interferon-alpha (IFN-alpha 2) binding determinants of the type I interferon receptor subunit IFNAR-1 with human/bovine IFNAR- 1 chimeras. *Biochemistry*, **37**, 13003–13010.
20. Cutrone, E. C. & Langer, J. A. (2001). Identification of critical residues in bovine IFNAR-1 responsible for interferon binding. *J. Biol. Chem.* **276**, 17140–17148.
21. Arduini, R. M., Strauch, K. L., Runkel, L. A., Carlson, M. M., Hronowski, X., Foley, S. F. *et al.* (1999). Characterization of a soluble ternary complex formed between human interferon-beta-1a and its receptor chains. *Protein Sci.* **8**, 1867–1877.
22. Wells, J. A. (1996). Binding in the growth hormone receptor complex. *Proc. Natl Acad. Sci. USA*, **93**, 1–6.
23. Letzelter, F., Wang, Y. & Sebald, W. (1998). The interleukin-4 site-2 epitope determining binding of the common receptor gamma chain. *Eur. J. Biochem.* **257**, 11–20.
24. Ozbek, S., Grotzinger, J., Krebs, B., Fischer, M., Wollmer, A., Jostock, T. *et al.* (1998). The membrane proximal cytokine receptor domain of the human interleukin- 6 receptor is sufficient for ligand binding but not for gp130 association. *J. Biol. Chem.* **273**, 21374–21379.
25. Livnah, O., Stura, E. A., Middleton, S. A., Johnson, D. L., Jolliffe, L. K. & Wilson, I. A. (1999). Crystallographic evidence for preformed dimers of erythropoietin receptor before ligand activation. *Science*, **283**, 987–990.
26. Bernat, B., Pal, G., Sun, M. & Kossiakoff, A. A. (2003). Determination of the energetics governing the regulatory step in growth hormone-induced receptor homodimerization. *Proc. Natl Acad. Sci. USA*, **100**, 952–957.
27. Remy, I., Wilson, I. A. & Michnick, S. W. (1999). Erythropoietin receptor activation by a ligand-induced conformation change. *Science*, **283**, 990–993.
28. Grotzinger, J. (2002). Molecular mechanisms of cytokine receptor activation. *Biochim. Biophys. Acta*, **1592**, 215–223.
29. Krause, C. D., Mei, E., Xie, J., Jia, Y., Bopp, M. A., Hochstrasser, R. M. & Pestka, S. (2002). Seeing the light: preassembly and ligand-induced changes of the interferon gamma receptor complex in cells. *Mol. Cell Proteomics*, **1**, 805–815.
30. Lenaz, G. (1987). Lipid fluidity and membrane protein dynamics. *Biosci. Rep.* **7**, 823–837.
31. Piehler, J. & Schreiber, G. (2001). Fast transient cytokine-receptor interactions monitored in real time by reflectometric interference spectroscopy. *Anal. Biochem.* **289**, 173–186.
32. Poo, H., Krauss, J. C., Mayo-Bond, L., Todd, R. F., 3rd & Petty, H. R. (1995). Interaction of Fc gamma receptor type IIIB with complement receptor type 3 in fibroblast transfectants: evidence from lateral diffusion and resonance energy transfer studies. *J. Mol. Biol.* **247**, 597–603.
33. Lim, J. K., Xiong, J., Carrasco, N. & Langer, J. A. (1994). Intrinsic ligand binding properties of the human and bovine alpha- interferon receptors. *FEBS Letters*, **350**, 281–286.
34. Frank, S. J. (2002). Receptor dimerization in GH and erythropoietin action–it takes two to tango, but how? *Endocrinology*, **143**, 2–10.
35. Sebald, W. & Mueller, T. D. (2003). The interaction of BMP-7 and ActRII implicates a new mode of receptor assembly. *Trends Biochem. Sci.* **28**, 518–521.
36. Gent, J., Van Den Eijnden, M., Van Kerkhof, P. & Strous, G. J. (2003). Dimerization and signal transduction of the growth hormone receptor. *Mol. Endocrinol.* **17**, 967–975.
37. Cunningham, B. C., Ultsch, M., De Vos, A. M., Mulkerrin, M. G., Clauser, K. R. & Wells, J. A.

(1991). Dimerization of the extracellular domain of the human growth hormone receptor by a single hormone molecule. *Science*, **254**, 821–825.
38. Takaoka, A., Mitani, Y., Suemori, H., Sato, M., Yokochi, T., Noguchi, S. *et al.* (2000). Cross talk between interferon-gamma and -alpha/beta signaling components in caveolar membrane domains. *Science*, **288**, 2357–2360.
39. Pearce, K. H., Jr, Cunningham, B. C., Fuh, G., Teeri, T. & Wells, J. A. (1999). Growth hormone binding affinity for its receptor surpasses the requirements for cellular activity. *Biochemistry*, **38**, 81–89.
40. Whitty, A., Raskin, N., Olson, D. L., Borysenko, C. W., Ambrose, C. M., Benjamin, C. D. & Burkly, L. C. (1998). Interaction affinity between cytokine receptor components on the cell surface. *Proc. Natl Acad. Sci. USA*, **95**, 13165–13170.
41. Piehler, J. & Schreiber, G. (1999). Biophysical analysis of the interaction of human ifnar2 expressed in *E. coli* with IFN alpha 2. *J. Mol. Biol.* **289**, 57–67.
42. Schmitt, H. M., Brecht, A., Piehler, J. & Gauglitz, G. (1997). An integrated system for optical biomolecular interaction analysis. *Biosens. Bioelectron.* **12**, 809–816.
43. Piehler, J., Brecht, A. & Gauglitz, G. (1996). Affinity detection of low molecular weight analytes. *Anal. Chem.* **68**, 139–143.
44. Piehler, J., Brecht, A., Valiokas, R., Liedberg, B. & Gauglitz, G. (2000). A high-density poly(ethylene glycol) polymer brush for immobilization on glass-type surfaces. *Biosens. Bioelectron.* **15**, 473–481.
45. Brian, A. A. & McConnell, H. M. (1984). Allogeneic stimulation of cytotoxic T cells by supported planar membranes. *Proc. Natl Acad. Sci. USA*, **81**, 6159–6163.
46. Piehler, J., Brecht, A., Giersch, T., Hock, B. & Gauglitz, G. (1997). Assessment of affinity constants by rapid solid phase detection of equilibrium binding in a flow system. *J. Immunol. Methods*, **201**, 189–206.
47. Axelrod, D., Koppel, D. E., Schlessinger, J., Elson, E. & Webb, W. W. (1976). Mobility measurement by analysis of fluorescence photobleaching recovery kinetics. *Biophys. J.* **16**, 1055–1069.

Edited by I. Wilson

(Received 26 January 2004; received in revised form 14 May 2004; accepted 17 May 2004)